PAPER

Pressure-driven collective growth mechanism of planar cell colonies

To cite this article: Claus Metzner *et al* 2018 *J. Phys. D: Appl. Phys.* **51** 304004

View the article online for updates and enhancements.

Pressure-driven collective growth mechanism of planar cell colonies

Claus Metzner[1,5] , Janina Lange[2], Patrick Krauss[3], Nico Wunderling[4], Julian Übelacker[1], Florian Martin[1] and Ben Fabry[1]

[1] Biophysics Group, Friedrich-Alexander-University, Erlangen, Germany
[2] Soft Condensed Matter Group, Ludwig-Maximilians-University, Munich, Germany
[3] Experimental Otolaryngology, University Hospital Erlangen, Erlangen, Germany
[4] Potsdam Institute for Climate Impact Research, Potsdam, Germany

E-mail: claus.metzner@gmail.com

Abstract
The growth of cell colonies is determined by the migration and proliferation of the individual cells. This is often modeled with the Fisher–Kolmogorov (FK) equation, which assumes that cells diffuse independently from each other, but stop to proliferate when their density reaches a critial limit. However, when using measured, cell-line specific parameters, we find that the FK equation drastically underestimates the experimentally observed increase of colony radius with time. Moreover, cells in real colonies migrate radially outward with superdiffusive trajectories, in contrast to the assumption of random diffusion. We demonstrate that both dicrepancies can be resolved by assuming that cells in dense colonies are driven apart by repulsive, pressure-like forces. Using this model of proliferating repelling particles, we find that colony growth exhibits different dynamical regimes, depending on the ratio between a pressure-related equilibrium cell density and the critial density of proliferation arrest.

Keywords: cell colonies, cell proliferation, cell–cell interactions, Fisher–Kolmogorov equation

S Supplementary material for this article is available online

(Some figures may appear in colour only in the online journal)

1. Introduction

The growth and self-organization of multicellular aggregates is of fundamental importance in morphogenesis [4, 5], wound healing [2, 4, 15, 18] and tumor development [4–6]. These processes typically involve different cell types interacting with each other and with a heterogeneous extracellular matrix. To simplify this complex situation, we here study the two-dimensional, radial-symmetric growth of tumor cell colonies, in which all cells are of the same lineage. Within this minimalistic framework, we ask a simple question: is it possible to predict the collective growth of the colony radius over time from measured single-cell properties, in particular from the density-dependent proliferation and migration behaviour of the cells?

To answer this question, we start out with the traditional Fisher–Kolmogorov (FK) equation [12]. This model assumes

a logistic, self-limiting proliferation of the cells, and thereby accounts for the known phenomenon of contact inhibition [1, 13, 16]. We measure the density-dependent proliferation rates for two exemplary cell lines (HT1080, which shows a saturating proliferation at large densities, and MCF7, which shows proliferation arrest beyond some critial density), and feed them into the FK equation. Strikingly, we find that the simulated colony radius is growing at a drastically smaller rate than in corresponding experiments. A subsequent theoretical analysis shows that this quantitative mismatch arises because the FK equation describes cell migration by free random diffusion, whereas cells in real colonies experience steric hindrance in regions of large density [9–11]. The direct effect of steric hindrance are pressure-like, repulsive forces that drive cells apart and thus accelerate the area growth of the colony. At the same time, this self-regulatory mechanism helps to keep the local cell density at a sufficiently low level, so that cells can continue to proliferate even deep within the colony.

---

[5] Author to whom any correspondence should be addressed.

1

J. Phys. D: Appl. Phys. **51** (2018) 304004

C Metzner *et al*

To account for pressure-driven cell transport, we develope a new model of proliferating repelling particles (PRP) that assumes short-range repulsive forces between nearby cells. We demonstrate that in combination with the measured density-dependent proliferation rate, this new transport mechanism reproduces the large measured growth rates of HT1080 and MCF7 colonies.

Moreover, the PRP model explains another surprising finding of the experiments: Even within the confluent cell sheet of a growing colony, cells are migrating radially outward with a superdiffusive mean squared displacement versus lag-time. This almost deterministic motion directly reflects the pressure gradients that build up within the colony.

Finally, we show that the PRP model can describe two distinct modes of colony growth, namely a 'linear' and a 'super-linear' regime. Whether a given cell type will end up in one or the other regime is determined by the dimensionless ratio between two key parameters of the system: the 'equilibrium' cell density ρ_{rep}, where the repulsive pressure just becomes zero, and the crital density of proliferation arrest ρ_{arr}.

The super-linear regime applies to cells with sufficiently large repulsion ($\rho_{rep} < \rho_{arr}$, case of MCF7) that reduce their local density to a sub-critical value by pushing their neighbors away, so that proliferation and streaming remain possible througout the whole colony. The same regime applies to cell types without any growth arrest, such as HT1080.

By contrast, the linear regime applies to cell types with proliferation arrest but weak repulsion ($\rho_{rep} > \rho_{arr}$) that proliferate until their density reaches the crital value ρ_{arr}, eventually leading to a static lattice of cells within the colony. In this growth regime (which resembles the predictions of the FK equation) proliferation is possible only at the colony border, and colony growth is generally slow.

2. Methods

(1) **Cell culture.** HT1080 fibrosarcoma cells were purchased from ATCC (#CCL-121) and cultured in Advanced DMEM F12 medium (#3133116000-028, gibco), supplemented with 5% FCS (fetal calf serum, #16000036, gibco) and 1% PSG (penicillin-streptomycin-glutamine, #10378016, gibco). MCF-7 mammary gland adenocarcinoma cells were also purchased from ATCC (#HTB-22). They were cultured in DMEM ($1\,g\,l^{-1}$ glucose, #31885-023, gibco), supplied with 10% FCS and 1% PSG. All lines were kept and imaged at 37 °C and 5% CO_2. Trypsin-EDTA (0.25%, #T3924, Sigma-Aldrich) was used for routine passaging of cells every third day.

(2) **Colony growth essay.** Prior to measurements, 15 000 cells were seeded into circular holes (diameter 4 mm) of a PDMS membrane, attached to a cell culture-treated petri dish. Before usage, membranes were coated with Pluronic F1127 (#P2443, Sigma-Aldrich) to avoid cell attachment. Over 24 h, the cells formed a monolayer. 2 h prior to the beginning of time-lapse measurements, membranes were removed and the cell monolayers could spread freely in all dimensions.

(3) **Measuring colony geometry.** The 2D projection of the colony shape was reconstructed by segmentation and thresholding analysis of phase contrast images. In addition, the 3D surface of the colonies was extracted from confocal fluorescent image stacks, after staining the fixed colonies with Draq5 (#DR05500, Biostatus).

(4) **Measuring cell migration within colonies.** Cells were placed in a microscope incubation chamber (37 °C, 5% CO_2), and phase contrast images were recorded for 24 h at 5 × magnification with interbvals of $\delta = 3$ min . Fluorescence images were taken in parallel, imaging fibronectin-coated fluorescent beads (#F8820, Invitrogen) of 1 μm diameter which were internalized by the cells. Bead tracking was used to reconstruct individual cell tracks. From the tracks, we computed the mean squared displacement versus lag-time, $\overline{\Delta r^2}(\tau) = \left\langle \left(\vec{r}_{t+\tau}^{(c)} - \vec{r}_t^{(c)} \right)^2 \right\rangle_{t,c}$, where $\vec{r}_t^{(c)}$ is the position of cell c at time t, and the average $\langle \ldots \rangle_{t,c}$ is over all times and cell indices. We also computed for each time point and cell within the field of view the angles of the cell displacements with respect to the radial direction of the circular colony, defined as $\Phi_{rad,t}^{(c)} = \text{angle}\left\{ (\vec{r}_{t+\delta}^{(c)} - \vec{r}_t^{(c)}),\ (\frac{\vec{r}_t^{(c)}}{|\vec{r}_t^{(c)}|}) \right\}$, and its distribution $p(\Phi_{rad})$.

(5) **Measuring density-dependent proliferation.** Each of the two cancer cell lines (MCF7 and HT1080) were seeded on Nunc dishes (area $9.6\,cm^2$) with three different starting numbers of cells: $1 \cdot 10^5$, $3 \cdot 10^5$, and $6 \cdot 10^5$. Cells were fixed and stained with Hoechst 33258 (Sigma-Aldrich) at 30 h, 54 h, 78 h and 102 h after seeding. Cells were counted using ClickPoints software [7].

(6) **Measuring density-dependent diffusion.** Each of the two cancer cell lines (MCF7 and HT1080) were seeded at two different densities, $2.09 \cdot 10^4\ cm^{-2}$ and $4.17 \cdot 10^5\ cm^{-2}$ in 4-compartment cell culture dishes, using three different dishes for each cell type and starting cell density. We measured cell diffusion after 24 h, 48 h, and 72 h. Three hours before starting the measurement, we added fluorescent beads to the cell samples. Images of the cells and beads were taken every three minutes with an exposure time of 5 ms for brightfield images and 100 ms for fluorescence images. Bead trajectories were measured with ClickPoints software.

(7) **Solving the radial-symmetric FK equation.** The radial-symmetric version of the FK equation (8) can be written as

$$\frac{d}{dt}\rho(r) = B(\rho) + \left(\frac{d\rho(r)}{dt} \right)_{dif}. \tag{1}$$

To solve it numerically, the simulated colony was divided into concentric rings of equal widths Δr, so that ring $k \in \{0, 1, \ldots\}$ was in between the radii $r_k = k\Delta r$ and r_{k+1}. Within each ring k, the particle density ρ_k was assumed to be constant. A discretization of the above partial differential equation yields

$$\frac{\Delta \rho_k}{\Delta t} = B(\rho_k) + \left(\frac{\Delta \rho_k}{\Delta t} \right)_{dif}, \tag{2}$$

where Δt is the simulation time step. The diffusion term was approximated by

$$\left(\frac{\Delta \rho_k}{\Delta t}\right)_{dif} \approx \frac{1}{r_k} \frac{(r_k I_{k-1}) - (r_{k+1} I_k)}{\Delta r}, \qquad (3)$$

where the diffusion current density between the boundary between rings k and $k+1$ was approximated as

$$I_k = \frac{D(\rho_k) + D(\rho_{k+1})}{2} \cdot \frac{\rho_k - \rho_{k+1}}{\Delta r}. \qquad (4)$$

(8) Quantitative argument against the border growth mechanism. A simple order-of-magnitude calculation shows that the fast growth of cell colonies cannot be based on diffusive migration. For this purpose, we consider the limiting case of the border growth regime, in which a mono-cellular layer of new cells is added to the circular outer border of the colony in regular time steps T_{lay}. This time step can be estimated from the observed radial growth rate of colonies ($\frac{dR_{col}}{dt} \approx 1$ mm/day) and the typical cell size ($L \approx 10$ μm) as $T_{lay} = L/\frac{dR_{col}}{dt} \approx 14.4$ min. All cells in the new layer must be produced by proliferation. Because a typical cell cycles takes about one day, $T_{div} \approx 24$ h, the probability that any cell in the colony divides during the layer adding time T_{lay} is only $p = T_{lay}/T_{div} \approx 0.01$. This in turn means that for each cell in the new layer, about 100 already existing cells are required to assure timely reproduction. Thus, at least the outermost 100 cell layers in a colony are responsible to produce, just in time, all the new cells needed for sustained linear colony growth. Yet, a new daughter cell produced at a distance $d = 100 * L \approx 1$ mm from inside the colony border also has to travel to the outer border within T_{lay}. If diffusion is the only transport mechanism for cells, and the typical experimentally observed diffusion constant is $D \approx 1$ μm^2 min^{-1}, a distance of $d = 1$ mm cannot be traveled in $T_{lay} = 14.4$ min. Rather, a realistic diffusion distance would be only $r_{dif} = \sqrt{4DT_{lay}} \approx 7.6$ μm. Even if new-born cells would migrate radially outward in a ballistic way, the required migration speed would be $v = \frac{1 \ mm}{14.4 \ min} \approx 66$ μm min^{-1}, which is unrealistic.

(9) Parameters of the PRP model. PRP simulations were performed as described in section 3.6. In each time step, the overdamped equations of motion for all particles were numerically solved by Euler forward integration with a fixed time increment $\Delta t = 1$ min, which was beforehand tested to be small enough to yield stable results. Cell radii were $r_C = 13.8$ μm (MCF7) and $r_C = 15.0$ μm (HT1080), according to our measurements on isolated cells that were adhering to the substrate. For both cell types, we used a detection radius of $r_B = 2r_C$ to determine the local density, a repulsive force range of $r_M = 2r_C$, and a repulsion strength parameter of $\kappa = 10/min$. The proliferation was set according to the respective measured functions $B(\rho)$. No Gaussian random shifts were added to the particle positions.

3. Results

3.1. Experiments with planar tumor cell colonies

In this paper, we focus on two exemplary cell lines: the mesenchymal-like fibrosarcoma line HT1080, and the epithelial-like breast adenocarcinoma line MCF7. Starting from a circular colony seed with a radius of 2 mm, we monitor the growth of the colonies over several days and measure the colony radius as a function of time (figure 1(d)). Furthermore, we follow the migration path of individual cells within the colony (figure 1(b)). The main findings are as follows:

(1) The outline of the colony border remains circular during the whole observation period (insets of figure 1(d)). The colonies have at any time a flat, dome-like shape, with a radius-to-height ratio of more than 100 (data not shown). They can therefore be approximated as two-dimensional objects, although cells eventually start to pile up into several layers in the most dense parts at the center of the colony. Consequently, the colony can be described by a two-dimensional cell density distribution, obtained by projecting all cell centers onto the growth plane.

(2) The colonies are densely packed sheets of cells and remain confluent during the entire growth process (figure 1(a)). In all parts of the colony except at the very border, cells are in direct contact with their neighbors. Only a few cells manage to escape from the colony for a short time.

(3) Over the measured time span of four days, the colony radius increases at an almost constant rate (figure 1(d)).

(4) The trajectories of individual cells within the colony appear like random walks. However, in particular close to the colony border, these random walks have a directional trend that is pointing radially outward (figures 1(b) and (c)).

(5) The mean squared displacement of the individual cell (pooled over the whole colony) grows with lag-time approximately as a power-law with a fractional exponent between one and two, indicating super-diffusive migration (figures 1(e) and (f)).

3.2. Traditional Fisher Kolmogorov (FK) equation

A natural way to model the growth of cell colonies is by reaction-diffusion equations [12], in particular by the FK equation:

$$\frac{d}{dt}\rho(x,t) = \beta(1-\rho)\,\rho + D\frac{\partial^2}{\partial x^2}\rho. \qquad (5)$$

This partial differential equation describes the changes of the position- and time-dependent cell density distribution $\rho(x,t)$ due to proliferation (first term on the r.h.s.) and migration (second term on the r.h.s.). To account for the effect of contact inhibition (which is known to exist for many cell types), the traditional FK equation assumes that the effective proliferation rate $\beta(1-\rho)$ decreases as a function of local cell density, up to the point of complete proliferation arrest (at $\rho = 1$
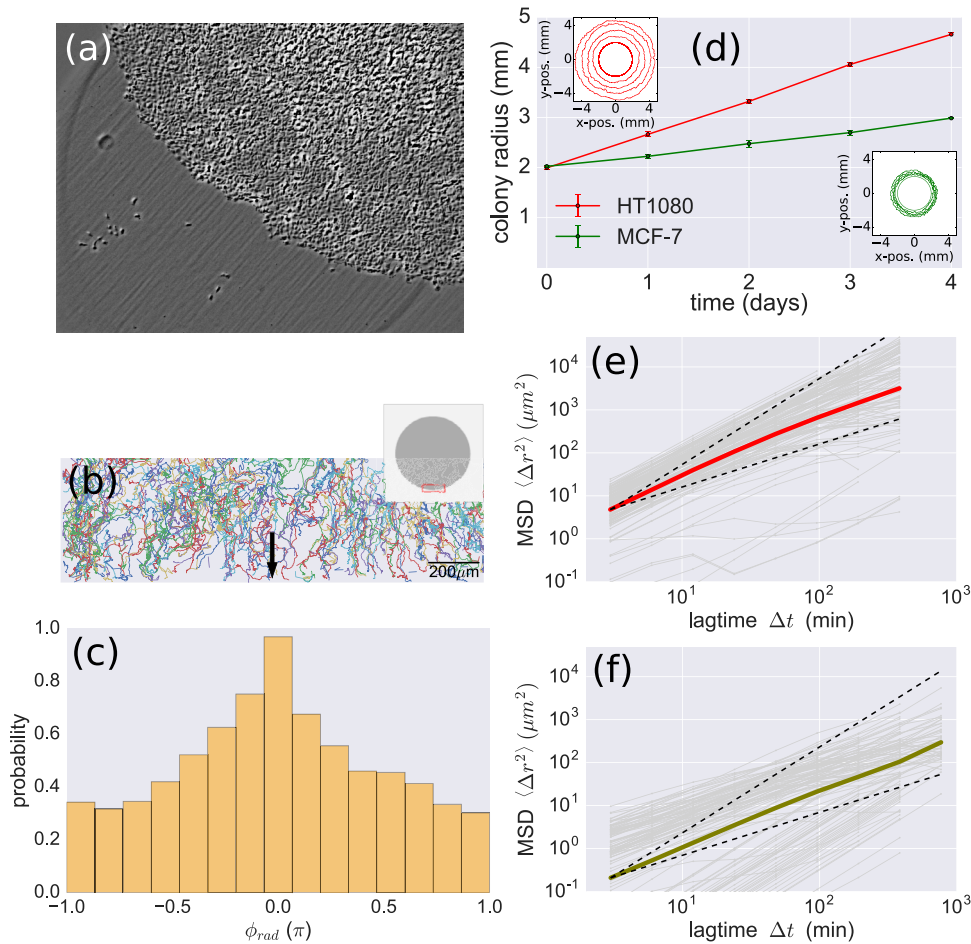
Figure 1. Experimental results from HT1080 and MCF7 cell colonies. (a) Outer section of a HT1080 colony after several days of growth. Cells are densely packed, and only few are found outside the colony. (b) Cell trajectories in an outer section (see inset) of the HT1080 colony. The main migration direction is radially outward (black arrow, pointing downward). (c) Distribution of the radial angle for the cells shown in b, showing a clear peak at $\Phi_{rad} = 0$, the radially outward direction. (d) Colony radius as a function of growth time for HT1080 (red) and MCF7 (green). The insets show the outlines of the colonies at each day. (e) Mean squared displacements of HT1080 cells versus lag-time, for some individual cells (light gray curves) and averaged over the population (thick red line). Dashed lines indicate the limits of diffusive and ballistic motion. The average MSD is superdiffusive. (f) Same as (e), but for MCF7 cells.

in the simple model presented here). Cell migration, on the other hand, is assumed to be independent from the cell density and is described by linear diffusion with a fixed diffusion constant D.

The above FK equation is often used to mimik the growth of a radial-symmetric 2D cell colony in one spatial dimension (here the x − coordinate). To describe experiments that start with a sub-confluent cell sheet, the equation is initialized with a density distribution $\rho(x, t = 0) < 1\ \forall x$ (left blue line in figure 2) that remains well below the critical density $\rho = 1$ of proliferation arrest, even at the dense center of the colony at $x = 0$. The FK equation then predicts that the subsequent colony growth will pass through two phases. In a first (transient) phase, both the spatial width of the cell density distribution and its maximum value increase over time in a non-linear manner. In the second (stationary) phase, the distribution attains a shape characterized by an inner plateau (where the density is pinned to the maximum possible value $\rho = 1$) and a border zone (where the density smoothly drops to zero). Over

time, the width of the density plateau is growing at a constant rate, while the border zone remains form-invariant.

This prediction, in particular the asymptotically linear growth of colony width over time, is indeed compatible with our data. However, in order to facilitate a *quantitative* comparison, the FK model must be adapted to the 2D, radial-symmetric geometry of our experiments. In addition, the idealized proliferation and migration terms of the traditional FK equation must be replaced by measured, cell-type specific expressions.

3.3. Density-dependent proliferation and diffusion

For this purpose, we first investigate the proliferation behavior of MCF7 and HT1080 cells in populations with a spatially homogeneous density $\rho(x, y) = \rho = const$ (see Methods). As a function of ρ, we measure the change rate $B(\rho) = \frac{d}{dt}\rho(x, t)|_{prol}$ of cell density due to proliferation (figure 3(a)). For MCF7 cells, we find that the proliferation function $B(\rho)$ first grows
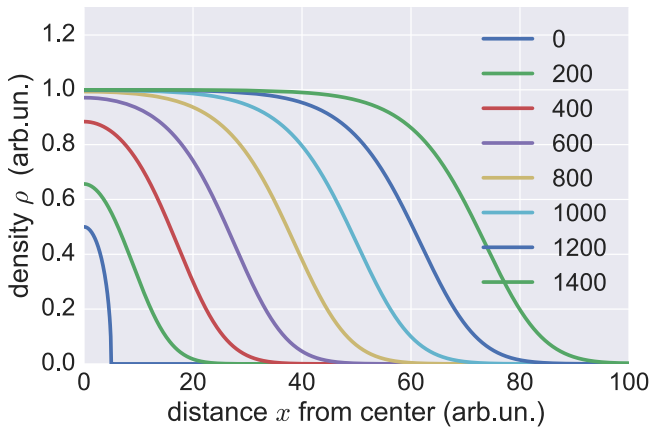
Figure 2. Solution of the traditional FK equation with a diffusion constant $D = 1$ and a prefactor $\beta = 0.1$ of the logistic proliferation term. The curves show, for 8 different time points (0–1400), the simulated cell density ρ as a function of the distance x to the center of a mirror-symmetric, one-dimensional 'colony'. Both density and position are in dimensionless units, with $\rho = 1$ correponding to the critial density of complete proliferation arrest.

with the density, but then decreases to zero beyond some critical value ρ_{arr}:

$$B_{\text{MCF7}}(\rho) = a\rho^2(\rho_{arr} - \rho)\,\theta(\rho_{arr} - \rho), \qquad (6)$$

where $a = 1.2 \cdot 10^2 \ \mu\text{m}^4 \ \text{min}^{-1}$, $\rho_{arr} = 4.5 \cdot 10^{-3} \ \mu\text{m}^{-2}$, and $\theta()$ is the Heaviside step function. Thus, as assumed in the logistic model of the traditional FK equation, MCF7 cells feature a growth arrest, although for small densities the proliferation function increases quadratically instead of linearly. For HT1080 cells, we find a qualitatively different behavior: proliferation increases monotonously and then saturates at some maximum value for very large densities:

$$B_{\text{HT1080}}(\rho) = b(1 - e^{-\rho/\rho_{sat}}), \qquad (7)$$

with $b = 1.6 \cdot 10^{-6} \ \mu\text{m}^{-2} \ \text{min}^{-1}$ and $\rho_{sat} = 2.1 \cdot 10^{-3} \ \mu\text{m}^{-2}$.

We also measure the average diffusion constant $D(\rho)$ as a function of the global cell density ρ in spatially homogenous populations (figure 3(b)). For MCF7 cells, we find a density-independent diffusion constant $D_{\text{MCF7}} = 0.185 \ \mu\text{m}^2 \ \text{min}^{-1}$, in agreement with the assumptions of the traditional FK equation. For HT1080 cells, we find a weak but nonetheless surprising *increase* of the diffusion constant with density that could be fitted linearly as $D_{\text{HT1080}}(\rho) = \alpha + \beta\rho$, with $\alpha = 0.86 \ \mu\text{m}^2$ min^{-1} and $\beta = 150 \ \mu\text{m}^4 \ \text{min}^{-1}$. We therefore conclude that cells do not experience contact inhibition of locomotion at the density range investigated in our experiments.

3.4. Cell-type specific FK equations

Next, we adapt the classical FK equation to the specific cell types MCF7 and HT1080, in order to test if the FK model is also *quantitatively* consistent with the measured properties of real cell colonies. For this purpose, the FK equation is extended to describe 2D, radial symmetric density distributions, where the density $\rho(r, t)$ depends only the radial coordinate (distance from the colony center) r and on time t. In general, this modified FK equations reads
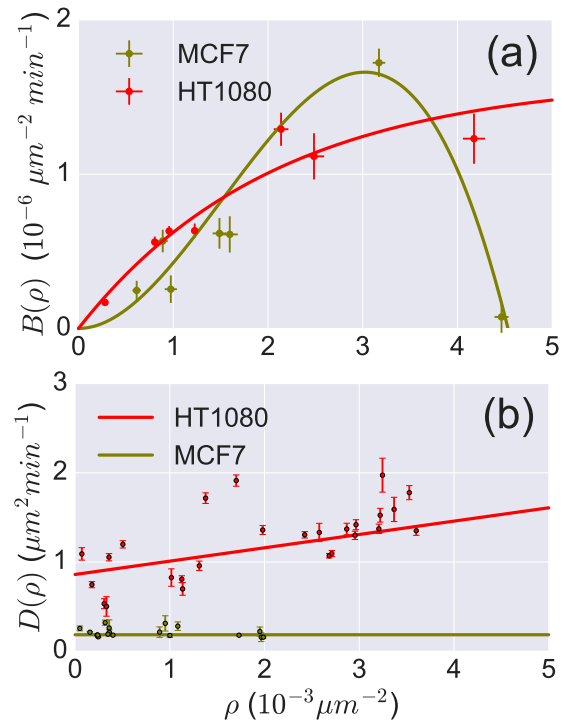

Figure 3. Measured proliferation rate and diffusivity (error bars and dots) of MCF7 cells (olive) and HT1080 cells (red) as a function of cell density ρ, as well as fit functions (solid lines). (a) The proliferation function $B(\rho)$, indicating the increase rate of local cell density due to cell divisions. For MCF7 cells, we used the fit function $a\rho^2(\rho_{arr} - \rho)\,\theta(\rho_{arr} - \rho)$. For HT1080 cells, we used the fit function $b(1 - e^{-\rho/\rho_{sat}})$ (b) The linear diffusivity $D(\rho)$ of cells. We find a constant diffusivity for MCF7 and a density-dependent diffusivity according to the linear fit $\alpha + \beta\rho$ for HT1080.

$$\frac{d}{dt}\rho(r, t) = B(\rho) + \frac{1}{r}\frac{\partial}{\partial r}\left[rD(\rho)\frac{\partial}{\partial r}\rho\right]. \qquad (8)$$

For $B(\rho)$ and $D(\rho)$, we insert the measured proliferation functions and diffusion constants of MCF7 and HT1080 cells, respectively. We then solve the cell-type specific equations numerically, starting with a disk-like initial density distribution that resembled the actual experimental situation.

For MCF7 cells (figure 4, left column), which feature density-independent diffusion and a proliferation arrest beyond some critical density, we recover the prediction of the traditional FK equation: a 'box-like' density distributions of fixed plateau value and linearly growing width (figure 4(a)). However, the width of the simulated distribution is growing at a drastically smaller rate than measured (figure 4(g)). We can reproduce the fast colony growth observed in the experiments only by artificially multiplying the measured diffusion constant by a factor of 81 (dashed line in figure 4(g)).

For HT1080 cells (figure 4, right column), which feature a diffusion constant that is slightly increasing with density and a proliferation that saturates at large densities, the cell-type specific FK equations show a different behavior: over time, the 'box-like' density distribution is now increasing both in height and width. Nevertheless, the simulated rate of colony
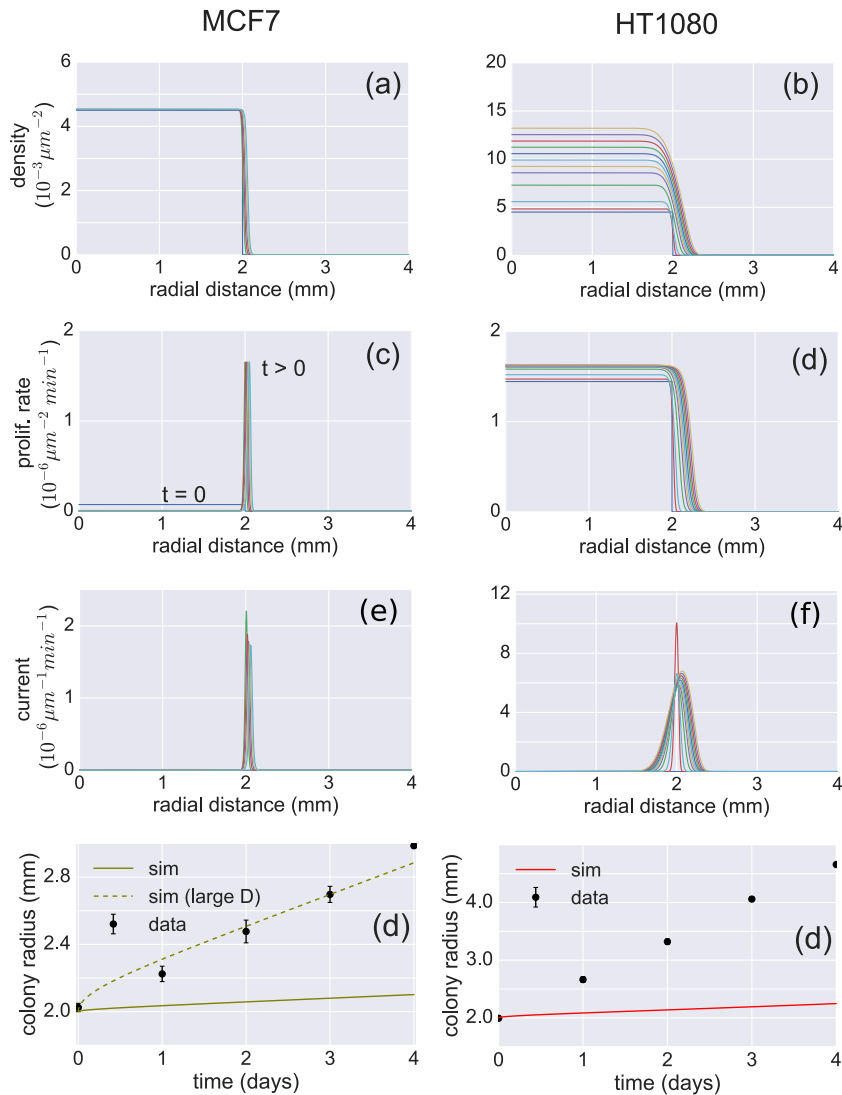
Figure 4. Simulated colony growth of MCF7 cells (left column) and HT1080 cells (right column), using cell-type specific FK equations with realistic, measured parameters. Rows show the cell density ((a) and (b)), the local proliferation rate ((c) and (d)), the diffusion current as functions of the distance from the colons center ((e) and (f)), and ((g) and (h)) the colony radius as a function of time as simulated (solid lines) and as measured in the experiments (dots with error bars). The growth rate is dramatically underestimated by the simulations. It starts to resemble the measured values (dashed line in (g)) only if the diffusion constant is artificially increased (by a factor of 81 in the case of MCF7).

growth (figure 4(h)) is—again—dramatically slower than in the corresponding experiments.

In addition to the cell density distributions, we also compute the local proliferation rates, as well as the local diffusion currents in the cell-type specific FK equations. For MCF7 cells, both the simulated proliferation rate (figure 4(c)) and the diffusion current (figure 4(e)) show extremely sharp peaks at the colony border, a feature *not* observed in the experiments. For HT1080 cells, the peak of the simulated diffusion current (figure 4(f)) has a somewhat more realistic width, and the simulated proliferation rate (figure 4(d)) is non-zero throughout the colony. Although we do not quantify proliferation in our HT1080 experiments, we indeed observe cell divsion events not only at the border of the colony, but also deep within. Nevertheless, the large discrepancy between the simulated and measured colony growth rates points to a fundamental

difference between the assumptions of the FK equation and the growth mechanism in real cell colonies.

3.5. Break-down of the FK equation

The problem with the FK equation can be seen most clearly in the example of MCF7 colonies, where the width of the border zone is extremely small in the simulations, leading to correspondingly narrow peaks of the proliferation rate and the diffusion current. Since proliferation and diffusion are the only microscopic processes that can increase colony size, all the colony growth has to be accomplished by this narrow border zone.

A simple estimation (see Methods (8)), using realistic cell parameters, demonstrates that this 'border growth mechanism' cannot generally be true: cell divisions happen much too infrequently in the border zone to generate all the new cells required

for the observed colony growth rates. Instead, colony growth must also rely on cell divisions that happen deep within the colony, but without requiring those new-born cells to migrate all the way to the colony border and attach there.

We therefore propose a collective colony growth mechanism that is driven by pressure: Directly after a cell-division, the total volume of the two daughters is equal to that of the mother cell, but the daughters will consume nutrients from the growth medium and finally regain their cell-type specific adult size. Since all cells in the dense bulk of the colony are in constant steric contact with their neighbors, this extra volume creates a pressure, which tends to drive the surrounding cells apart from the new-born cells. Once this pressure has relaxed and the average cell density is restored, the colony has necessarily expanded by a small amount. In other words, cell proliferation is continuously producing pressure gradients that are equilibrated by collective cell rearrangements, and this mechanism is mainly responsible for the expansion of the colony. In this new model, the collective outward streaming of cells (figures 1(b) and (c)) is interpreted as a pressure-driven, rather than an entropy-driven current.

3.6. PRP model

To study in detail the effects of pressure on the motion of individual cells within the colony, we implement a particle-based simulation model. In this model, particles are represented by their center position in the 2D plane. During each time step Δt, all particles have an opportunity to proliferate and to migrate, in a way that depends on their local neighbors.

Proliferation of a particle i can be described by a binary random variable $b_i \in \{0, 1\}$, where $b_i = 1$ means that the particle undergoes division in the present time step. The variable b_i could be any deterministic or stochastic function of the present (and past) state of i and its local environment. In our model, we set $b_i = 1$ with a probability $P_i = \Delta t \, B(\rho_i)/\rho_i$ that reflects the measured, density-dependent proliferation function $B(\rho)$. The local density $\rho_i = n_i/(\pi r_B^2)$ is determined by the number n_i of neighbors around particle i within a detection radius r_B. To model cell division in a simple way, we replace the mother particle by two daughter particles at (almost) the same position and assume that the daughters immediately have their adult size.

Migration of a particle i can be described by a shift of its position $\Delta \vec{r}_i$, which, again, could be any deterministic or stochastic function of the state of i and its local environment. In our model, we neglect all stochastic components and compute the shift $\Delta \vec{r}_i = \Delta t \, \vec{v}_i = \Delta t \, \vec{F}_i/\gamma$ as the motion of an over-damped particle under a total force $\vec{F}_i$, assuming an effective friction constant γ. This total force $\vec{F}_i = \sum_j \vec{f}_{ij}$ is modeled as a sum of two-particle forces $\vec{f}_{ij}$ between i and its neighbors j, within an interaction radius r_M. For simplicity, we assume purely repulsive, spring-like two-particle forces $|\vec{f}_{ij}| = k \left(1 - \frac{d_{ij}}{r_M}\right) \theta(1 - \frac{d_{ij}}{r_M})$, where k is the spring constant, $d_{ij} = |\vec{r}_i - \vec{r}_j|$ is the distance between i and j, and $\theta()$ is the Heaviside step function. Thus, the overall strength of the repulsion effect is controlled by the single parameter $\kappa = k/\gamma$.

3.7. Emergent features of the PRP model

To systematically explore the interplay of different model ingredients, we perform a series of five increasingly complex simulations, using idealized system parameters (see supplemental material (stacks.iop.org/JPhysD/51/304004/mmedia)). The main results are as follows:

(1) In a system without proliferation but with repulsive interactions (SM-figure 6), particles that were initially seeded as a very dense cluster are spreading out laterally and eventually form an approximately hexagonal lattice with a density of $\rho_{rep} = \frac{2}{\sqrt{3}r_M^2}$, determined by the interaction radius r_M. This self-organized lattice density ρ_{rep} is a dynamic key parameter of the system.

(2) When cell proliferation and repulsive interactions are simultaneously present, the behavior of the system depends on the relative size of the lattice density ρ_{rep} and the density ρ_{arr} of proliferation arrest. The case $\rho_{rep} > \rho_{arr}$ of strong (density-induced) inhibition of proliferation results in a linear growth regime, similar to the results of the FK equation (SM-figure 7): The colony radius is growing linearly with time, as proliferation occurs exclusively at the border of the colony, the only place where the local density ρ is smaller than ρ_{arr}. Particles inside the colony are effectively trapped within the hexagonal lattice, allowing only for sub-diffusive particle motion.

(3) The opposite case $\rho_{rep} < \rho_{arr}$ of weak inhibition of proliferation, which also applies to cell types that lack any growth arrest, results in a super-linear growth regime (SM-figure 8): The colony radius is increasing over time with larger and larger speed, and proliferation occurs all over the colony. The hexagonal lattice structure is lost, so that particles can move super-diffusively despite of the large density in the colony.

(4) In this super-linear growth regime, particles close to the colony border reach at some point unrealistically large velocities. Enforcing a speed limit v_{max} for the individual particle motion fixes this problem, but leads to qualitative changes of the colony dynamics (SM-figure 9): After a super-linear transient period corresponding to case (3), the colony radius keeps growing at a constant maximum rate $\frac{dR}{dt} \approx v_{max}$. Proliferation becomes enhanced at the colony border, but to a smaller extend also occurs throughout the bulk of the colony. Driven by the pressure forces, particles are streaming radially outward, leading to an almost ballistic motion.

(5) In the super-linear growth regime with speed limit, the colony dynamics does not qualitatively change when a modest diffusive (random) component is added to the motion of each particle (SM-figure 10): The average mean-squared displacement of particles remains super-diffusive and the colony radius is growing linearly once the speed limit is reached. The super-linear growth regime qualitatively reproduces all features observed in our experiments with MCF7 and HT1080 cells.
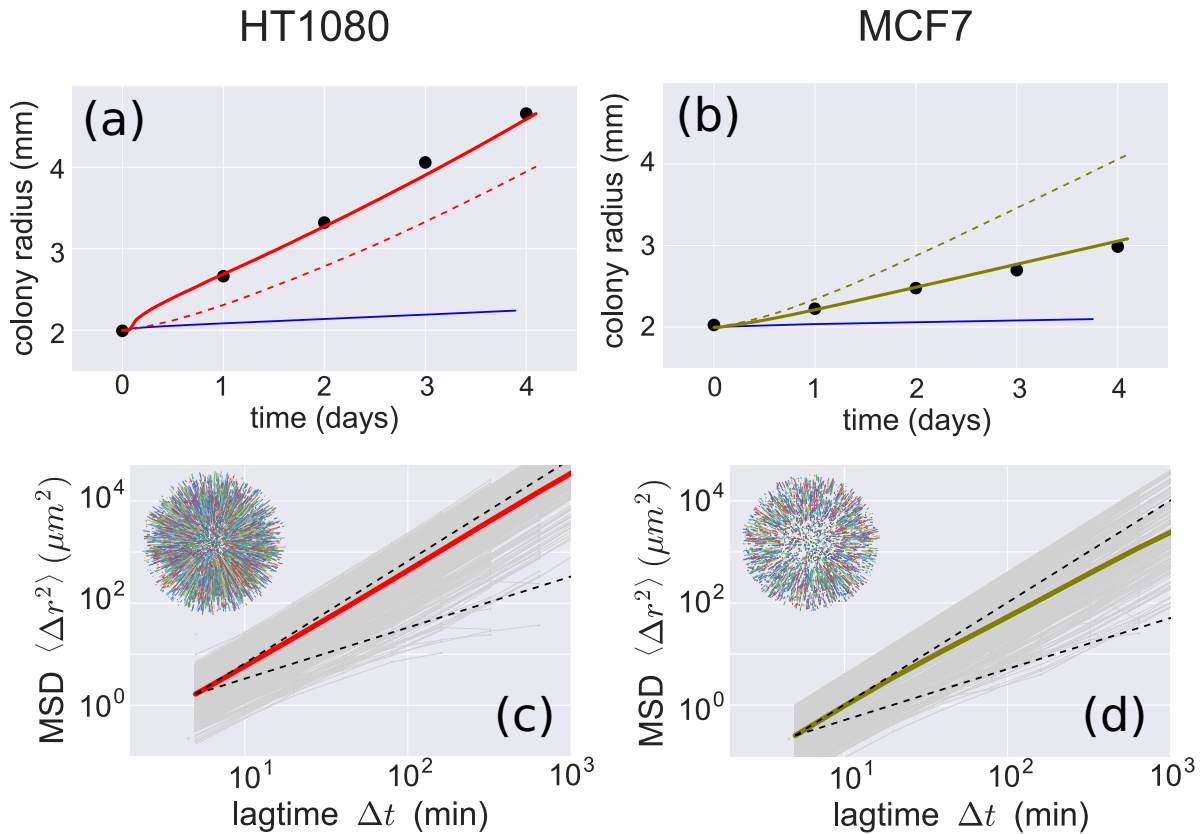
J. Phys. D: Appl. Phys. **51** (2018) 304004

C Metzner *et al*

HT1080

MCF7

Figure 5. Comparison of colony growth simulations (lines) with data (black dots), for HT1080 (left colomn) and MCF7 (right column). (a) Colony radius of HT1080 cells versus growth time according to the cell-specific FK equation (flat blue line), with the PRP model for a starting density of $\rho(t=0) = 1.0 \cdot \rho_{rep}$ (red dashed line), and with the PRP model for a starting density of $\rho(t=0) = 2.2 \cdot \rho_{rep}$ (thick red line). (b) Analogous to (a), however for MCF7 cells. Here, both PRP simulations were started with a pressure-free initial configuration, correponding to the density $\rho(t=0) = 1.0 \cdot \rho_{rep}$. One simulation allows for arbitrary migration speeds (olive dashed line), the other assumes a speed limit of 2 μm min^{-1}. (c) Simulated mean squared displacements of HT1080 cells versus lag-time (PRP model, same run as thick line in (a)), for some individual cells (light gray curves) and averaged over the population (thick red line). Dashed lines indicate the limits of diffusive and balistic motion. The average MSD is strongly superdiffusive. The inset shows the radial outward streaming of the individual cells within the colony. (d) Same as (c), but for MCF7 cells.

3.8. Cell-type specific PRP model

To test if the PRP model can also quantitatively replicate the experimentally measured colony growth rates, we insert the measured proliferation functions $B(\rho)$ of MCF7 and HT1080 cells into the PRP simulations. We assume reasonable values for repulsion strength and interaction radius that bring the system into the super-linear regime. Since random particle diffusion, as shown in the last section, has only a small effect on colony dynamics, we neglect this feature, thereby avoiding an additional simulation parameter.

We start the simulations with n_0 cells distributed uniformly within a circular area of 2 mm radius. This area is enclosed by a mechanical constriction, modelled by a spring-like container-force that points radially inward. Before releasing the constriction (realized by switching the spring-constant of the container abruptly to zero), cells are allowed to equilibrate for some period without proliferation, thus leading to a more regular, almost hexagonal lattice of cells. This emulates the starting situation in the actual colony experiments, where the cells were allowed to form a dense, mechanically relaxed layer for several hours prior to removing the constriction.

In a first simulation run, we set the initial number n_0 of cells to a value that correponds exactly to the 'equilibrium density' ρ_{rep}, so that there is no pressure in the colony prior to the simulated growth. At $t = 0$, the constriction force is switched off and proliferation is switched on. For this relaxed initial condition, we find that the simulated increase of colony radius over time has the same order of magnitude as in the experiments, both for HT1080 cells (figure 5(a), dashed line) and for MCF7 cells (figure 5(b), dashed line). However, the PRP simulations slightly under-estimate the measured colony growth rate in the case of HT1080 (figure 5(a), black dots) and slightly over-estimate it in the case of MCF7 (figure 5(b), black dots).

Since we did not measure the exact cell density at $t = 0$ in the experiments, we tested if the small remaining mismatch between HT1080 simulations and data may be attributed to differences in the initial conditions. When we assume that the initial density was $2.2 \cdot \rho_{rep}$ rather than $1.0 \cdot \rho_{rep}$, the colony starts already with a certain degree of pressure. This initial pressure speeds up colony growth, and we indeed obtain an almost perfect agreement with the measurements (figure 5(a), solid red line).

In the case of MCF7, the experimentally observed colony growth is smaller than in the simulations, which may simply reflect the natural speed limit of MCF7 cells for collective migration. If we introduce a speed limit of 2 μm min^{-1}, we also obtain an almost perfect agreement with the measurements (figure 5(b), solid olive line).

Finally, we investigate the trajectories of the cells during the simulated colony growth. Both for HT1080 (figure 5(c), solid red line) and for MCF7 (figure 5(d), solid olive line), we obtain highly super-diffusive mean squared displacements versus lag-time, reflecting the radially outward directed streaming of the cells (see insets of figures 5(c) and (d)). Although the super-diffusive cell motion observed in the experiments (figures 1(e) and (f)) is less pronounced, presumably due to additional random motions that are neglected in the simulations, this agreement suggests that pressure-gradients can give rise to deterministic, radially outward directed cell streaming.

4. Discussion

In this paper, we have demonstrated that repulsive cell–cell interactions explain, both, the fast growth of planar HT1080 and MCF7 colonies, as well as the superdiffusive streaming of the cells from inside the colony towards its border. Striving for the simplest model that is compatible with our data, we have neglected certain bio-physical aspects that are known to play an important role in the behavior of other multicellular aggregates.

In particular, we have neglected any adhesive cell–cell interactions, which could lead to the formation of long-range tensile stresses within the colony [17]. In principle, such adhesive interactions would enable a subset of 'leader cells', located at the colony border and actively moving outward, to pull other cells behind, thereby contributing to colony growth by a different mechanism. Indeed, it has been shown that some biological tasks (such as tissue repair [8]) require both pulling and pushing of the cells [3]. With the two cell types ivestigated in this paper, however, we found no evidence of leader cells.

Another factor that can indirectly affect colony growth is the size available for cells at different positions in the colony. In particular, cells with the freedom to spread and polarize optimally will achieve larger migration speeds [14]. In our cell colonies, we indeed found that at the colony border, where cell density is lower, the average cell size is somewhat larger and simultaneously the speed of the radial outward motion of cells is faster. In a similar way, the opportunity of cells to spread may serve as a signal that regulates the cell cycle [3]. Although we did not explicitly account for cell-size dependent migration and proliferation in our simulations, we did so indirectly: The available space per cell is directly related to the local cell density, and we have measured quantitatively how this density controls the motility and division rate of the cells.

Finally, we did not take into account any explicit tendency of the cells to align their direction of motion with that of their nearest neighbors. As has been studied previously [19], such a tendency can lead to the emergence of long-range collective

streaming patterns in particle aggregates, just as we have observed them in our colonies. However, as we have demonstrated, the pressure gradients in a radial symmetric colony, combined with repulsive mechanical interactions of cells in steric contact, are sufficient to explain the outward directed streaming.

Acknowledgments

ORCID iDs

Claus Metzner https://orcid.org/0000-0002-5709-4306

References

[1] Brú A, Albertos S, Subiza J L, García-Asenjo J L and Brú I 2003 The universal dynamics of tumor growth *Biophys. J.* **85** 2948–61

[2] Brugués A, Anon E, Conte V, Veldhuis J H, Gupta M, Colombelli J, Muñoz J J, Brodland G W, Ladoux B and Trepat X 2014 Forces driving epithelial wound healing *Nat. Phys.* **10** 683–90

[3] Drasdo D and Hoehme S 2012 Modeling the impact of granular embedding media, and pulling versus pushing cells on growing cell clones *New J. Phys.* **14** 055025

[4] Friedl P and Gilmour D 2009 Collective cell migration in morphogenesis, regeneration and cancer *Nat. Rev. Mol. Cell Biol.* **10** 445–57

[5] Friedl P, Hegerfeldt Y and Tusch M 2004 Collective cell migration in morphogenesis and cancer *Int. J. Dev. Biol.* **48** 441–9

[6] Friedl P, Locker J, Sahai E and Segall J E 2012 Classifying collective cancer cell invasion *Nat. Cell Biol.* **14** 777

[7] Gerum R C, Richter S, Fabry B and Zitterbart D P 2017 Clickpoints: an expandable toolbox for scientific image annotation and analysis *Methods Ecol. Evol.* **8** 750–6

[8] Hoehme S *et al* 2010 Prediction and validation of cell alignment along microvessels as order principle to restore tissue architecture in liver regeneration *Proc. Natl Acad. Sci.* **107** 10371–6

[9] Lang N R, Skodzek K, Hurst S, Mainka A, Steinwachs J, Schneider J, Aifantis K E and Fabry B 2015 Biphasic response of cell invasion to matrix stiffness in three-dimensional biopolymer networks *Acta Biomater.* **13** 61–7

[10] Lange J R and Fabry B 2013 Cell and tissue mechanics in cell migration *Exp. Cell Res.* **319** 2418–23

[11] Lautscham L A *et al* 2015 Migration in confined 3d environments is determined by a combination of adhesiveness, nuclear volume, contractility, and cell stiffness *Biophys. J.* **109** 900–13

[12] Marel A-K, Zorn M, Klingner C, Wedlich-Söldner R, Frey E and Rädler J O 2014 Flow and diffusion in channel-guided cell migration *Biophys. J.* **107** 1054–64

[13] Mayor R and Carmona-Fontaine C 2010 Keeping in touch with contact inhibition of locomotion *Trends Cell Biol.* **20** 319–28

[14] Nasrollahi S, Walter C, Loza A J, Schimizzi G V, Longmore G D and Pathak A 2017 Past matrix stiffness

J. Phys. D: Appl. Phys. **51** (2018) 304004

C Metzner *et al*

primes epithelial cells and regulates their future collective migration through a mechanical memory *Biomaterials* **146** 146–55

[15] Poujade M, Grasland-Mongrain E, Hertzog A, Jouanneau J, Chavrier P, Ladoux B, Buguin A and Silberzan P 2007 Collective migration of an epithelial monolayer in response to a model wound *Proc. Natl Acad. Sci.* **104** 15988–93

[16] Puliafito A, Hufnagel L, Neveu P, Streichan S, Sigal A, Fygenson D K and Shraiman B I 2012 Collective and single

cell behavior in epithelial contact inhibition *Proc. Natl Acad. Sci.* **109** 739–44

[17] Trepat X, Wasserman M R, Angelini T E, Millet E, Weitz D A, Butler J P and Fredberg J J 2009 Physical forces during collective cell migration *Nat. Phys.* **5** 426

[18] Vedula S R K *et al* 2015 Mechanics of epithelial closure over non-adherent environments *Nat. Commun.* **6** 6111

[19] Vicsek T, Czirók A, Ben-Jacob E, Cohen I and Shochet O 1995 Novel type of phase transition in a system of self-driven particles *Phys. Rev. Lett.* **75** 1226